Stabilizing a severely deformed Al–7Mg alloy with a multimodal grain structure via Mg solute segregation

Min Zha[a,b,c], Hong-Min Zhang[b], Xiang-Tao Meng[b], Hai-Long Jia[b,c], Shen-Bao Jin[e], Gang Sha[e], Hui-Yuan Wang[a,b,c*], Yan-Jun Li[d*], Hans J. Roven[d]

[a]*State Key Laboratory of Superhard Materials, Jilin University, Changchun, 130012, PR China*

[b]*Key Laboratory of Automobile Materials of Ministry of Education & School of Materials Science and Engineering, Nanling Campus, Jilin University, No. 5988 Renmin Street, Changchun 130025, PR China*

[c]*International Center of Future Science, Jilin University, Changchun 130012, PR China*

[d]*Department of Materials Science and Engineering, Norwegian University of Science and Technology, 7491 Trondheim Norway*

[e]*Department of Materials Science and Engineering, Nanjing University of Science and Technology, Nanjing 210094, China*

Abstract

Single-phase Al–Mg alloys processed by severe plastic deformation (SPD) usually suffer from unsatisfactory thermal stability at moderate to high temperatures with recrystallization occurring and obvious grain coarsening. In the present work, an Al–7Mg alloy prepared by equal-channel angular pressing (ECAP) possessed markedly enhanced thermal stability upon annealing at moderate to high temperatures (200–275 ºC), compared with those ultrafine-grained dilute Al–Mg alloys with a uniform microstructure. The enhanced thermal stability is due primarily to the multimodal grain structure consisting of nano-, ultrafine- and micron-sized coarse grains, strong segregation and/or clusters of Mg solute along grain boundaries (GBs), and Al_3Mg_2 precipitates formed during annealing. First, extensive recovery predominates over recrystallization and consumes most of stored energy in the ECAPed Al–7Mg alloy annealed at ≤ 275 ºC, leading to the recrystallization and growth of nano/ultrafine grains being retarded or postponed. Moreover, Mg solute segregation and/or clusters along GBs of nano/ultrafine grains could further suppress grain growth via diminishing GB energy and dragging GBs efficiently. In addition, Al_3Mg_2 precipitates formed with increasing annealing time could inhibit grain growth by pinning GBs. The present multimodal-grained Al–7Mg alloy with enhanced thermal stability is believed to be particularly attractive in potential engineering applications at moderate to high temperatures.

* Corresponding author. Tel/fax: +86 431 8509 4699

E–mail address: wanghuiyuan@jlu.edu.cn (Hui-yuan Wang); yanjun.li@ntnu.no (Yan-jun Li)

Keywords*:* Al–Mg alloys; ECAP; Multimodal grain structure; Solute segregation; Thermal stability

1. Introduction

Al–Mg alloys possess good formability, high specific strength, excellent corrosion resistance and so on, which makes them highly desirable for commercial applications [1–5]. It has been found that increasing Mg addition favours dislocation accumulation by strong interactions with dislocations and more importantly can decrease the stacking fault energy of Al alloys, which is beneficial to generating submicron- or nano-sized grains via severe plastic deformation (SPD) [6,7]. Due to high-volume fraction grain boundaries (GBs), however, poor thermal stability in nano/ultrafine-grained alloys prepared by SPD has always been an issue [8–10], e.g. single-phase dilute Al–Mg alloys exhibited strong susceptibility to coarsening even at 200 ^{o}C [11,12]. Several strategies have been proposed to improve the poor thermal stability of nano/ultrafine-grained alloys, which can be classified into two categories, i.e. kinetic stabilization and thermodynamic stabilization strategies [7,13–15]. The kinetic stabilization is to retard GB mobility by solute drag [7], second-phase particle pinning [12] and so on. The thermodynamic stabilization is realized via reducing GB energy, e.g. by solute segregation [8,16].

Both experimental results and simulation studies have proved that Mg atoms tend to segregate along GBs in Al alloys [17–21]. Moreover, higher Mg concentrations represent larger driving force for the decomposition of Al–Mg supersaturated solid solution, which can promote strong Mg segregation [1]. For example, the Mg concentration of segregation layers in an as-sputtered nanocrystalline Al–10Mg (at.%) alloy, i.e. 20 at.%, is far higher than 5.5 at.% in Al–5Mg [22]. Although the strong Mg segregation along GBs leading to improved grain coarsening resistance has been demonstrated in as-sputtered films [22], the scale of as-sputtered films is too small (e.g. 100 nm in thickness) towards industrial applications.

In the case of decomposition, even partial, significant mobility of Mg atoms is required. Therefore, in addition to the level of Mg solute in the matrix [1], the GB segregation of Mg depends primarily on concentrations of vacancy and dislocation greatly [6,3]. During SPD, the Mg mobility could be enhanced dramatically, attributed to (i) high-concentration vacancies [1] and/or (ii) high-density dislocations via pipe diffusion mechanism or solute drag provided dislocation velocity is lower than the critical value [16,23]. Under the flux of vacancies and/or dislocations towards GBs acting as sinks, Mg atoms tend to redistribute with a large possibility for forming Mg segregation [23]. Besides, special GBs in non-equilibrium configuration tend to form during SPD and are extremely unstable owing to intrinsic characteristics of excess GB energy, long range elastic stresses and enhanced free volume [23]. Nevertheless, Mg segregation relaxes partial elastic strains via inducing local compressive stresses and hence stabilizes these special GBs by reducing GB energy [23].

Preparing bimodal/multimodal grain structures gains great attention due to the advantage in achieving high strength and ductility simultaneously [24]. For example, our previous work reported a superior strength-ductility synergy, i.e. tensile strength of ~600 MPa and uniform ductility of ~14%, in a bulk multimodal-grained high solid solution Al–7Mg alloy processed by equal-channel angular pressing (ECAP) [25]. However, the thermal stability and high-temperature application of bimodal-/multimodal-grained materials have been rarely reported. Distinct recovery and recrystallization behaviours are expected in such bimodal/multimodal grain structures, in comparison to unimodal nano-/ultrafine-grained Al–Mg alloys, because of differences in GB characteristics and dislocation densities among grains with different size scales. Till now, few studies concern the synergistic effects of Mg solute segregation and a bimodal/multimodal grain structure on thermal stability of high solid solution Al–Mg alloys.

Herein, we utilized a high Mg concentration to achieve a multimodal grain structure and strong Mg segregation along GBs in an ECAPed Al–7Mg alloy. This research aims at

providing a fundamental understanding of the improved thermal stability in the Al–7Mg alloy. It is believed that the present study is of great technological importance for potential applications of high-strength and ductile high solid solution bulk Al–Mg alloys at moderate to high temperatures.

2. Experimental procedures

The binary Al–7Mg cast ingot was supplied by Hydro Aluminum, with chemical compositions of 7.0 Mg, 0.05 Fe, 0.06 Si and Al in balance (wt.%), as measured by optical emission spectrometry (OES). Bars with 100×19.5×19.5 mm^3 in dimension, cut from ingots, were homogenized at 500 °C for 3 h. Thereafter, ECAP combined with inter-annealing at 300 °C for 120 s between selected passes was performed at room temperature with route Bc, using a 90° die, till 5 passes. The detailed ECAP route can be referred to [25,26]. Uniformly deformed regions from the normal and extrusion direction (i.e. ND-ED plane) were cut for subsequent microstructure observations and hardness measurements. Isothermal annealing treatments were performed in an air furnace when annealed at ≤ 275 °C or molten salt bath furnace when annealed at 300 °C for short time.

Transmission electron microscopy (TEM) foils were processed by twin-jet electro polishing in a solution of 33% nitric acid in methanol at -30 °C. TEM detection was carried out on a Philips CM30 at 150 kV and JEM-2100F at 200 kV. The TEM orientation mapping was performed employing a JEOL ARM200CF at 200 kV equipped with the Nanomegas ASTAR system. Samples for X-ray diffraction (XRD) and electron backscatter diffraction (EBSD) detection were prepared by standard metallographic routes and then were electro polished in a solution of 80% C_2H_5OH + 20% $HClO_4$ at 20 V for 15–25 s at -30 °C. XRD was performed on a Siemens D5000 at 40 kV, Cu K_α radiation, with a step size of 0.02° and 20 s/step. Furthermore, EBSD detection was undertaken on a Zeiss 55VP FEG-SEM equipped with a Nordif EBSD detector and TSL OIM software, performing at 20 kV, 20 mm working

distance, 70° tilt, and 0.05–0.1 μm scan step depending on magnifications. More details about the grain construction procedure during EBSD analyses are available in [27].

The tip samples with a cross-section of 0.5×0.5 mm^2 for atom probe tomography (APT) characterization were prepared by a two-step electro-polishing procedure. Samples were first electrolyzed in a solution of 25% perchloric acid in acetic acid at 15 V and room temperature and then electrolyzed in a solution of 4% perchloric acid at 20 V. APT detection was carried out using a local electrode atom probe (LEAP 4000X Si) at 26 K with 568 nm laser wave length, at pulse-laser energy of 100 PJ and with a target evaporation rate of 1%. Vickers microhardness measurements were studied under a 200 g load applied for 15 s. At least eight separate measurements were conducted for each condition.

3. Results

3.1 The as-ECAPed microstructure

3.1.1 Grain structure

A representative EBSD map, showing the initial microstructure after homogenization at 500 °C for 3 h, reveals that the Al–7Mg alloy consists of uniform coarse grains with an average size of ~100 μm before ECAP (Fig. 1(a)). However, due to the low intensity of Kikuchi diffraction patterns caused by the large retained stress, EBSD investigation on SPD-processed Al–Mg alloys with ≥ 5 wt.% Mg is very difficult [28]. Herein, TEM using Nanomegas-ASTAR was performed to reveal the microstructure of present as-ECAPed Al–7Mg alloy. The TEM-ASTAR image indicates many equiaxed nano and ultrafine grains together with a considerable fraction of slightly larger elongated grains (~500 nm in width and ~1.5 μm in length) in the as-ECAPed sample (Fig. 1(b)), which is a typical bimodal grain structure, as further evidenced by the grain size distribution (Fig. 1(d)). Note that some areas predominated by much coarser grains may also exist, which cannot be covered by TEM images due to the limited area being observed. The corresponding kernel average

misorientation (KAM) map shown in Fig. 1(c) reveals that most of grains in the as-ECAPed Al–7Mg alloy, including nano/ultrafine grains, have similar degree of local internal strains. The geometrically necessary dislocation (GND) density estimated by $\rho_{GND} = 2\theta/ub$, based on the KAM map, is ~6.0×10^{15} m^{-2}, where $b = 2.86\times10^{-10}$ m is the Burgers vector for pure Al [27], θ is the local misorientation angle (in radians), u is the scanning step length [29]. The calculated GND density in the as-ECAPed sample is even higher than the total dislocation density values in Al–Mg alloys (with Mg contents ≤ 4.1 wt.%) processed by high-pressure torsion (HPT) and ECAP, i.e. ~$1.7–23\times10^{14}$ m^{-2} [30–32].

More careful observations find that nano and ultrafine grains are dominantly bounded by high angle grain boundaries (HAGBs) (Fig. 1(b)). However, the distribution of GB misorientation angles indicates that a sharp peak locates at low angle grain boundaries (LAGBs) of ~2° (Fig. 1(e)), which should mainly correspond to LAGBs developed in interiors of slightly larger elongated grains. To examine misorientation in them, misorientation profiles along lines of L1–L4 in Fig. 1(b) are shown in Fig. 2. One can see large accumulated misorientation gradients in the selected grains, i.e. 8–20 deg/μm. The GND density calculated by the misorientation profiles, based on $\rho \approx \theta/(b\delta)$, roughly is ~$7\times10^{15}$ m^{-2}, where θ is the accumulated misorientation angle (in radians) within a distance δ [27]. The calculated result from the misorientation profiles is similar to that obtained by the KAM map.

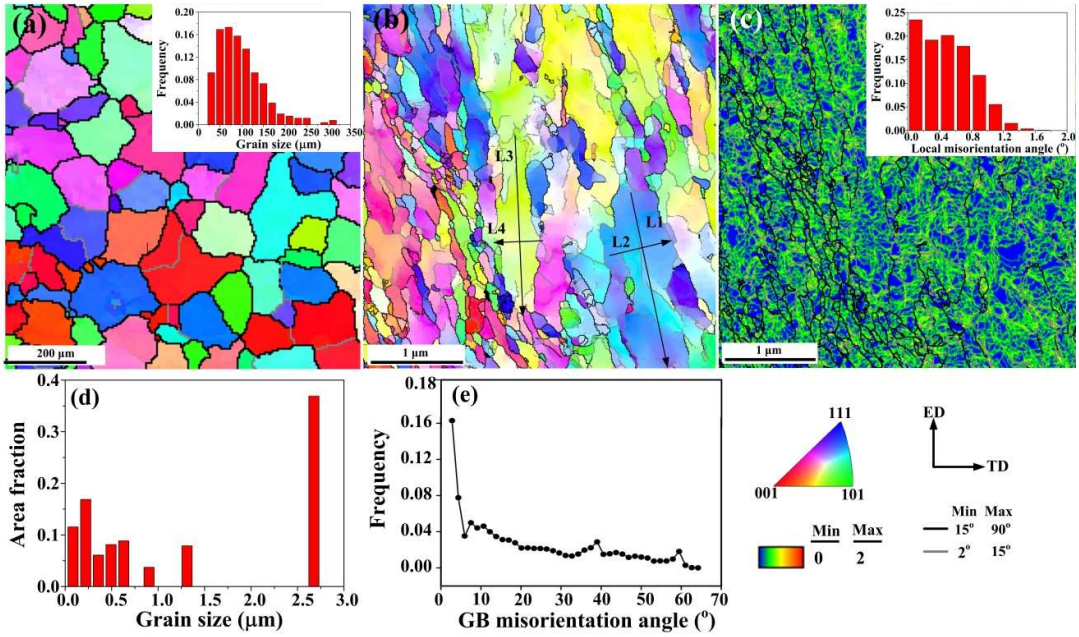

Fig. 1. (a) Representative EBSD map of the homogenized Al–7Mg alloy; (b) typical TEM-based orientation map (Nanomegas-ASTAR), (c) corresponding KAM map, (d) grain size distribution and (e) GB misorientation angle distribution of the as-ECAPed Al–7Mg alloy; insert in (a) and (c) is corresponding grain size distribution and local misorientation angle distribution, respectively, while the one in bottom right is the color coded map of crystal orientations parallel to ND.

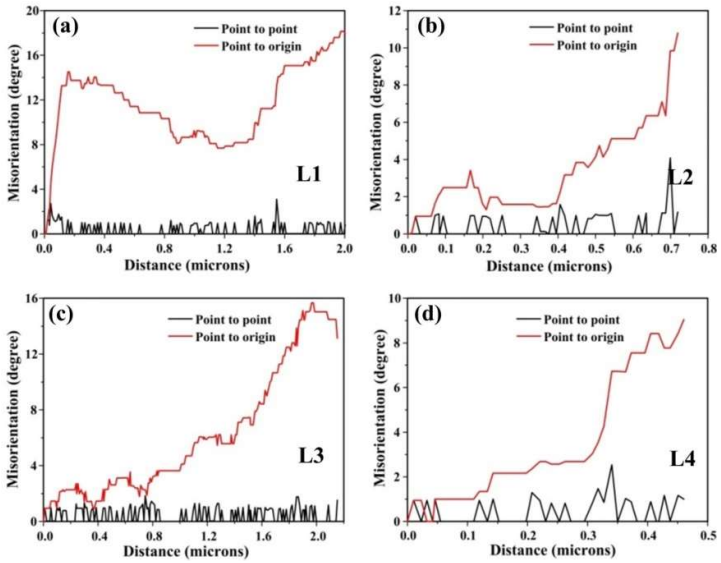

Fig. 2. Misorientation profiles measured along lines L1–L4 in Fig. 1(a). The black lines show point-to-point misorientation while the red lines show point-to-origin misorientation.

TEM images show a submicron-sized polycrystalline structure (Fig. 3). Ultrafine grains in an elongated shape, with ~50–100 nm in width and ~200–500 nm in length are observed, while others are equiaxed and even finer (< 100 nm) (Fig. 3(a)). A higher-magnification TEM

image reveals that GBs in elongated grains are often curved and poorly defined (e.g. GB1 and GB2), i.e. fuzzy GBs with a high level of internal stress and elastic distortion in the crystal lattice, indicative of the presence of non-equilibrium GBs (Fig. 3(b)). Besides, both TEM observations and selected area diffraction (SAD) pattern identify the absence of Mg-rich phases in present as-ECAPed high solid solution Al–7Mg alloy.

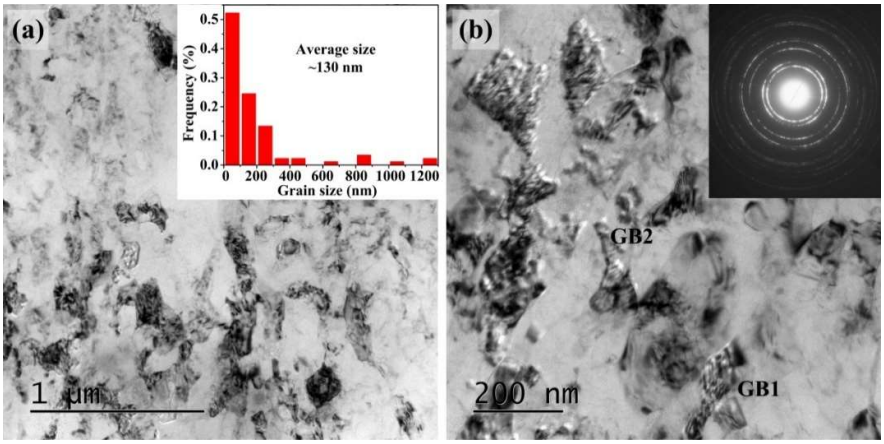

Fig. 3. Typical TEM images of the as-ECAPed Al–7Mg alloy. The insert in (a) and (b) is the corresponding grain size distribution and representative SAD pattern, respectively.

3.1.2 Mg distribution

XRD patterns of Al–7Mg samples in both as-homogenized and as-ECAPed conditions are presented in Fig. 4, showing only peaks of Al phase and no reflections of Mg- or Fe-containing compounds. A least squares refinement was done to evaluate lattice constants of both samples since peak shifts towards lower scattering angle are noticed, as compared to the theoretical diffraction peaks of pure Al. Table 1 records the lattice parameter and corresponding loss of Mg concentration in the as-ECAPed Al–7Mg sample, compared with the as-homogenized one (at 500 °C for 3 h). Considering the solid solubility of Mg in Al matrix at 500 °C, i.e. ~11 wt.% [33], it is assumed that almost all of Mg atoms are in solid solution in the as-homogenized sample. The slight decrease in lattice parameter of the as-ECAPed condition, relative to the as-homogenized condition, i.e. 4.0810±0.0001 Å *vs.*

4.0860±0.0002 Å, should result from the loss of ~0.96 wt.% Mg atoms, based on the fact that 1 at.% Mg leads to the change in lattice parameter by ~0.0046 [34].

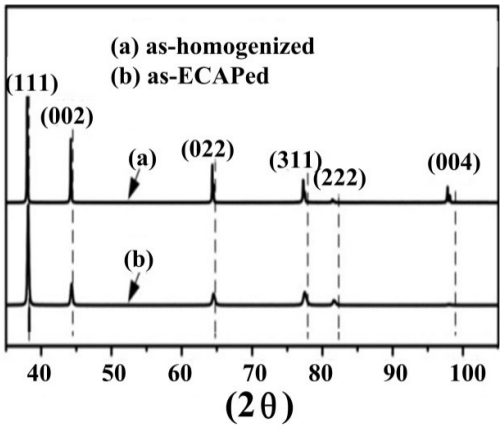

Fig. 4. XRD patterns of the Al–7Mg alloy: (a) in as-homogenized state and (b) in as-ECAPed state. For comparison, theoretical diffraction peak positions of pure Al (lattice constant a = 4.0412 Å [35]) are included and presented as vertical dotted lines.

APT analyses were carried out to further identify the distribution of solute Mg atoms. Fig. 5 displays atom maps of Al and Mg elements in the as-ECAPed sample. The analyzed volume clearly shows no obvious Mg concentration fluctuations in grain interiors (Fig. 5(a)). The local concentration of solute Mg measured by APT in a small volume is ~8.36 at.%, slightly larger than the actual Mg composition of ~7 wt.% (i.e. 7.8 at.%) obtained by OES in a bulk sample. It is reasonable that the local Mg concentration is higher than the bulk Mg concentration due to the general tendency of non-uniform distribution behaviors of Mg in SPD-processed Al–Mg alloys [6]. The concentration profile across GB1 reveals merely subtle fluctuations of Mg concentration (Fig. 5(b)) while the local Mg concentration is up to ~40 at.% within a layer of ~7–20 nm width at GB2 and GB3, indicating Mg segregation and/or clusters forming (Fig. 5(c–e)). The difference in segregation characteristics might depend on crystallographic characteristics of GBs and deformation mechanism during plastic proceeding process [6]. Also, strong Mg segregation was detected in a high-pressure torsion (HPT)-processed Al–5.8Mg alloy [1].

Well known is that the structural width of GBs is small. Even in the case of non-equilibrium GBs, the corresponding structural width is significantly smaller than 10 nm, which in general reaches a value of 1.5 to 2.0 nm [23]. Herein, it should be noted that the thickness of Mg-richened layer along GBs, i.e. 7–20 nm, does not necessarily represent the thickness of GBs. The Mg-richened layer could be thicker than GBs provided Mg solute atoms continuously diffuse into the already formed solute-richened layer with increasing ECAP passes and during inter-pass annealing process, forming a thick Mg cluster along GBs, as shown in Fig. 5(d). Normally, the formation of solute segregation or clusters along GBs can be explained by mechanical and thermal activation [36]. During SPD, the flux of dislocations and/or vacancies towards GBs tends to couple with Mg atoms, promoting the Mg redistribution and local enrichments [16,1,23]. Furthermore, thermal exposure during inter-pass annealing at 300 ºC in the present ECAP route, could guarantee Mg atoms with sufficient diffusion. Both factors contribute to strong Mg segregation and/or clusters along GBs in the as-ECAPed Al–7Mg alloy. Note that no Mg-enriched precipitates are detected either within grains or at GBs.

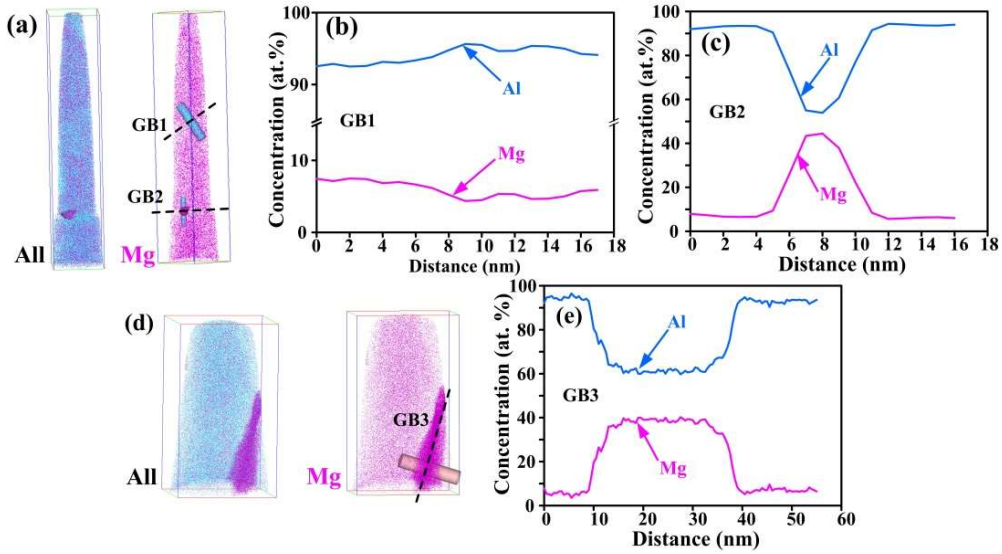

Fig. 5. APT analyses of the as-ECAPed Al–7Mg alloy: (a) and (d) element distribution maps, where Al (blue) and Mg (pink) atoms are clearly presented; (b), (c) and (e) concentration profiles showing local Mg distribution along GBs.

3.2 Annealing and recrystallization behaviors

3.2.1 Microhardness evolution

Microhardness values of present ECAPed sample undergone different annealing conditions are displayed in Fig. 6. Fig. 6(a) shows the dependence of hardness on temperature after annealing for 30 min. When annealed at 200 °C, a slight decrease in hardness from more than 200 Hv to ~180 Hv is seen. With increasing annealing temperature to 250 °C and further to 275 °C, the hardness decreases more evidently to ~140–150 Hv. One can see that upon extending annealing time to 24 h at 200 °C and to 8 h at 275 °C, the ECAPed sample is relatively stable without any obvious drop in hardness value (Fig. 6(b)). However, when annealed at 300 °C, the hardness decreases sharply in only a few minutes and then attains a plateau (Fig. 6(c)), indicating recrystallization occurs rapidly.

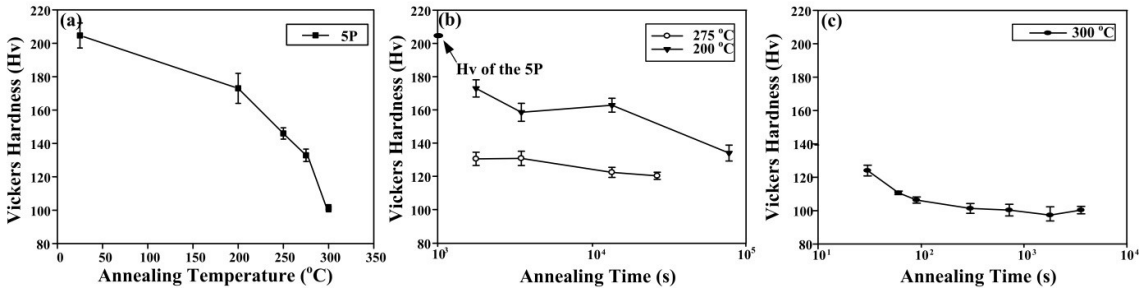

Fig. 6. Microhardness evolution of the ECAPed Al–7Mg alloy annealed at different conditions: (a) at various temperatures for 30 min, (b) at 200 and 275 °C with increasing time and (c) at 300 °C with increasing time.

3.2.2 Microstructural evolution during annealing

When annealed at 200 and 250 °C for 30 min, grain structure in the present ECAPed sample is still quite heterogeneous, i.e. a large number of necklace-like ultrafine equiaxed (sub) grains distributing along HAGBs of micron-sized coarse deformed grains (Fig. 7(a) and (b)). Information from Fig. 7 combined with results in Figs. 1 and 3 further confirms that a multimodal grain structure forms in the as-ECAPed sample where nano and ultrafine grains coexist with micro-sized coarse grains. With extending annealing time to 24 h at 200 °C,

extensive recovery occurs in micron-sized coarse grains with amounts of subgrains forming but the as-deformed multimodal grain structure is still retained (Fig. 7(c)).

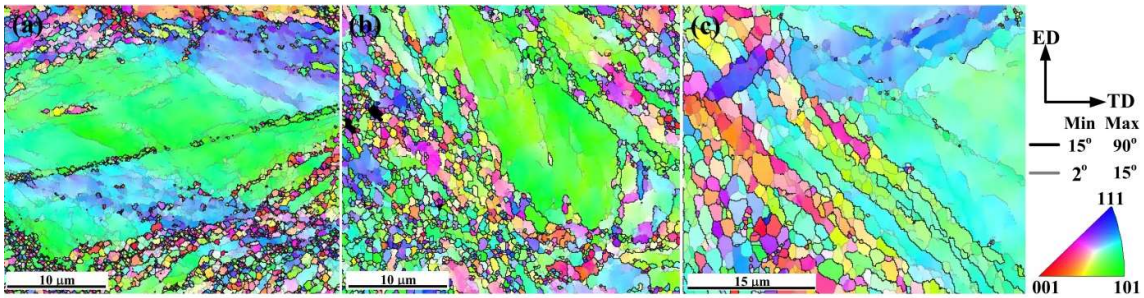

Fig. 7. Typical EBSD maps of the ECAPed Al–7Mg alloy annealed at: (a) 200 °C for 30 min, (b) 250 °C for 30 min and (c) 200 °C for 24 h. Insert in the bottom right is the color code of crystal orientations parallel to ND.

The grain structure annealed at 275 °C for 75 min becomes less heterogeneous (Fig. 8(a)), compared with samples annealed at 200 and 250 °C for 30 min (Fig. 7(a) and (b)). It is mainly because partial recrystallization occurs in coarse deformed grains with some new grains forming meanwhile original ultrafine/fine grains coarsen slightly after annealing at 275 °C for 75 min. With extending annealing time to 8 h, recrystallization is gradually expanded into coarse grains where well-arranged fine equiaxed grains are generated (Fig. 8(b)). Nevertheless, the existence of considerable subgrains indicates that extensive recovery still proceeds.

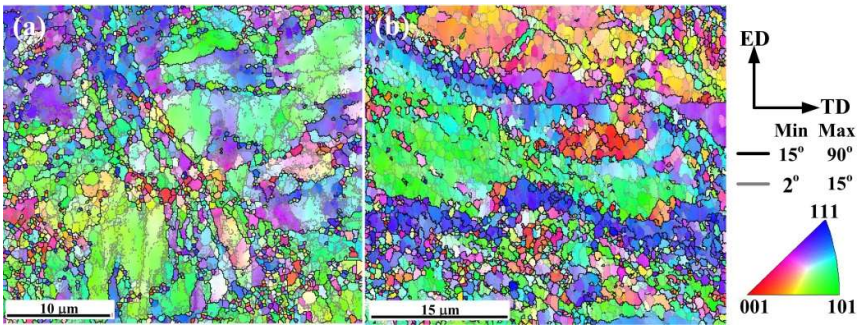

Fig. 8. Typical EBSD maps of the ECAPed Al–7Mg alloy annealed at 275 °C for (a) 75 min and (b) 8 h. Insert in the bottom right is the color code of crystal orientations parallel to ND.

Upon annealing at 300 °C for 30 s, recrystallization occurs and necklace-like ultrafine equiaxed grains form along band structure boundaries (Fig. 9(a)). The band structures tend to

align in parallel and intersect with others at localized zones. After annealing for 60 s, the band structures disappear, leaving the microstructure consisting mainly of recrystallized grains and some of them with large sizes (Fig. 9(b)). Upon extending annealing time to 300 s, recrystallization almost completes and more obvious grain growth occurs (Fig. 9(c)).

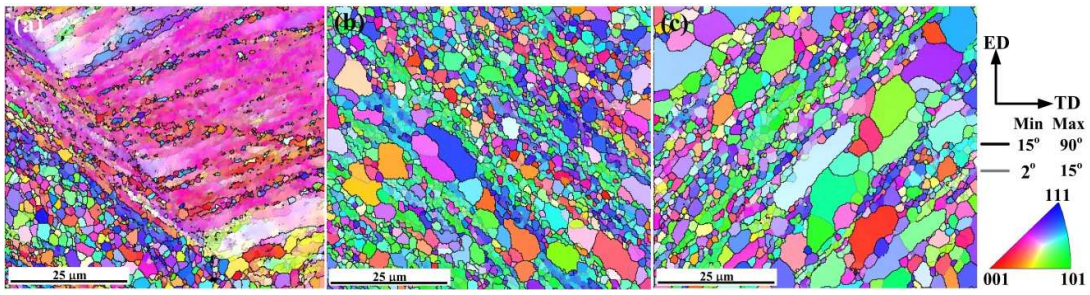

Fig. 9. Typical EBSD maps of the ECAPed Al–7Mg alloy annealed at 300 °C for (a) 30 s, (b) 60 s and (c) 300 s. Insert in the bottom right is the color code of crystal orientations parallel to ND.

XRD patterns of the ECAPed samples annealed at different conditions are shown in Fig. 10. Lattice parameters and corresponding loss of Mg concentration referred to the as-homogenized one are recorded in Table 1. Significant loss of Mg concentration, i.e. a decrease of 2.42 and 2.19 wt.% Mg atoms, occurs in samples annealed at 200 °C for 24 h and at 250 °C for 30 min, respectively. It may be due either to the strong Mg segregation and/or clusters along GBs or to the possibly formed precipitates. Upon annealing at 275 °C for 75 min, the Mg loss decreases, i.e. a reduction of 1.59 wt.% solute Mg is detected. However, after annealing at 300 °C for only 30 s, the lattice parameter approaches that in the as-homogenized sample, indicating nearly all Mg atoms are in solid solution, which is rationalized by the Mg equilibrium solubility of 7.2 wt.% at 300 °C [37].

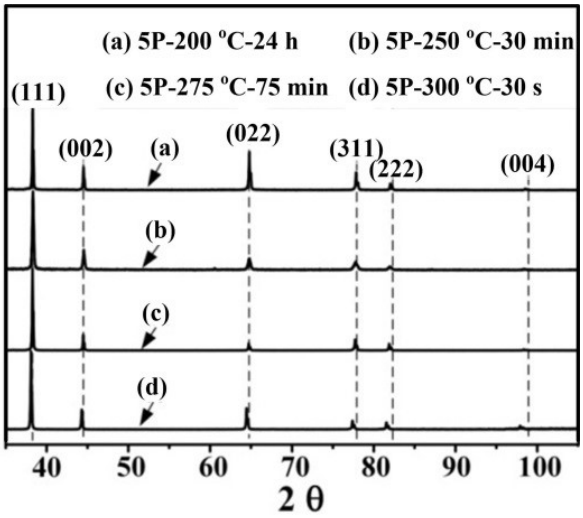

Fig. 10. XRD patterns of the ECAPed Al–7Mg alloy annealed at different conditions: (a) at 200 °C for 24 h, (b) at 250 °C for 30 min, (c) at 275 °C for 75 min and (d) at 300 °C for 30 s. For comparison, theoretical diffraction peak positions of pure Al (lattice constant a = 4.0412 Å) are included and presented as vertical dotted lines.

TEM observations were performed on both samples annealed at 250 °C for 30 min and at 200 °C for 24 h. Clearly, grains in the 250 °C-annealed sample are elongated and contain high-density dislocations (Fig. 11(a–c)). The average size of nano/ultrafine grains is ~170 nm (Fig. 11(a)), which is comparable to that in the as-ECAPed sample (~150 nm) (Fig. 3(a)). Moreover, no Mg-containing precipitates are observed (Fig. 11(b)). After annealing at 200 °C for 24 h, the microstructure is partially recrystallized and grains are mainly in two states, i.e. elongated deformed grains and fine equiaxed recrystallized grains (Fig. 11(d–f)), showing an average size of ~220 nm (Fig. 11(d)). It is noteworthy that some (sub) GBs are more likely pinned by newly precipitated nanoscale particles of 20–30 nm, indicated by arrows in Fig. 11(e) and (f). The inserted SAD in Fig. 11(e) demonstrates these fine particles are Al_3Mg_2. It indicates that Al_3Mg_2 phase tends to precipitate from the supersaturated Al matrix after long-time low-temperature annealing.

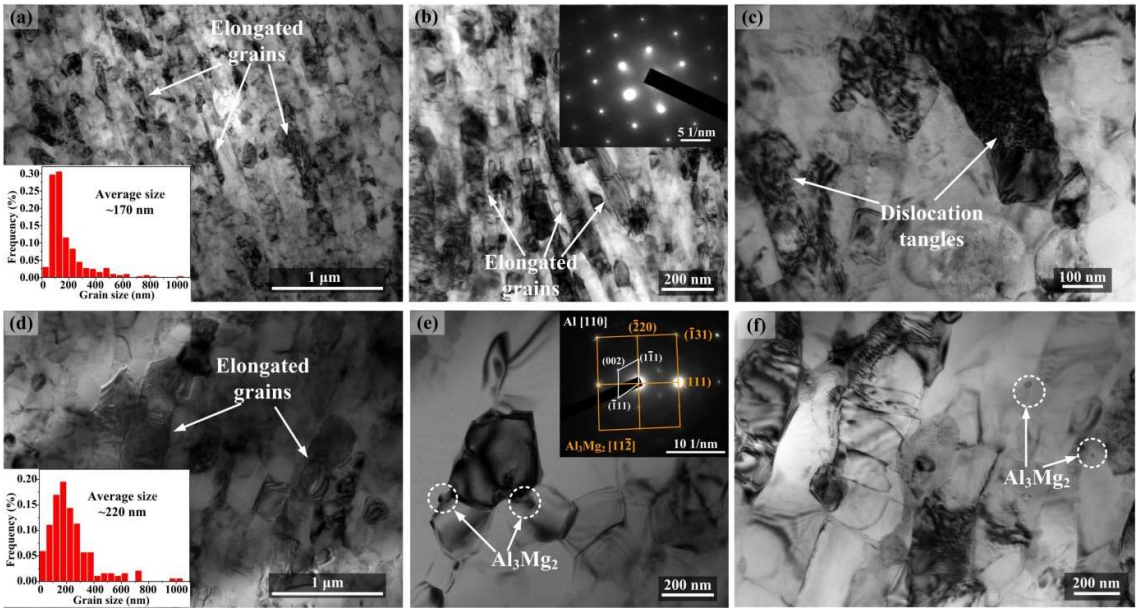

Fig. 11. TEM images of ECAPed samples annealed at: (a–c) 250 °C for 30 min and (d–f) 200 °C for 24 h. Inserts in (a) and (d) are corresponding grain size distribution charts while these in (b) and (e) are corresponding SAD patterns.

4. Discussion

The dilute ultrafine-grained ECAPed Al–Mg alloys usually possess low thermal stability [38,39]. However, due to the difficulty in preparing high solid solution Al–Mg alloys by multiple-pass ECAP at room temperature, investigations on their annealing behaviours and thermal stability are rare. Therefore, it is of great interest to evaluate the thermal stability at moderate to high temperatures of present multimodal-grained Al–7Mg alloy processed via ECAP.

The change in average grain size with annealing time at different temperatures is shown in Fig. 12(a). As expected, the grain growth rate rises with increasing temperatures. After annealing at 200 °C even for 24 h and at 275 °C for 8 h, Al–7Mg samples exhibit slight grain growth with average sizes < 1 μm. However, grains grow sharply and heterogeneously at 300 °C in extremely short time, e.g. 60 s, in the range of 1–20 μm. Nevertheless, the multimodal-grained Al–7Mg alloy displays enhanced thermal stability at ≤ 275 °C, compared to ECAPed pure Al and Al–3Mg, as well as cryo-rolled 5083 Al alloy, whose grains coarsened readily

when annealed at low temperatures for short time [12,38–40]. For example, the average grain size of an ECAPed Al–3Mg sample increased obviously from ~0.3 μm to ~0.8 μm upon annealing at 200 °C for 1 h [12]. Similarly, another ECAPed ultrafine-grained Al–3Mg alloy annealed at 250 °C for 1 h displayed recrystallization and a duplex structure, with grains coarsening to ~5–10 μm [38,39].

Herein, to evaluate the thermal stability of present multimodal-grained ECAPed Al–7Mg alloy, the variation in grain sizes is further analysed to calculate the corresponding grain growth exponent (n) at different temperatures (Fig. 12(b)). The n is normally obtained by the empirical equation [41,42]:

$$D^n - D_0^n = kt$$

where D and D_0 is the average instantaneous and initial grain size, respectively, t is the annealing time and k is a temperature-dependent constant. It is assumed that the role of stored energy on grain growth in the present study could be ignored since the extensive recovery during annealing consumes most of stored energy in both coarse grains and nano/ultrafine grains at moderate to high temperatures (≤ 275 °C). Thereby, the grain growth exponent of the multimodal-grained Al–7Mg alloy is deduced based on the assumption that the driving force on GB migration arises from the GB curvature [43]. Well known is that $n = 2$ is a reference value for pure metals or alloys annealed at very high temperatures [41]. The respective n value of ~3.9 and ~3.5 at 200 and 275 °C again proves enhanced thermal stability of the Al–7Mg alloy at moderate to high temperatures, i.e. ≤ 275 °C.

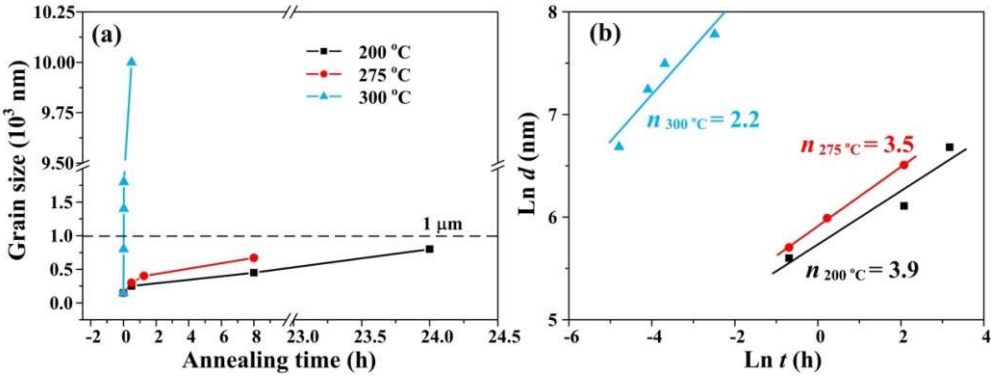

Fig. 12. (a) The change in average grain size with annealing time at 200–300 °C and (b) corresponding grain growth exponent at different temperatures.

The enhanced thermal stability of the ECAPed Al–7Mg alloy is partially attributed to the inherent multimodal grain structure. Well known is that recovery and recrystallization are competing processes as both are driven by stored energy [43–45]. When annealed at ≤ 275 °C, the driving force is insufficient to activate extensive recrystallization, and hence recovery predominates over recrystallization. Moreover, considerable subgrains have formed in annealed samples (Figs. 7 and 8), which is a typical character of the occurrence of extensive recovery. Furthermore, prior recovery is more likely to occur in coarse grains as a higher dislocation density, i.e. more stored energy exists in them than that of nano/ultrafine grains (Fig. 13). Accordingly, most of stored energy is consumed by extensive recovery, which in turn, decreases the tendency for nano/ultrafine grains to consume coarse grains through recrystallization. Thereby, the recrystallization and growth of nano/ultrafine grains in the multimodal-grained Al–7Mg alloy could be retarded or postponed to some degree when annealed at moderate to high temperatures (≤ 275 °C).

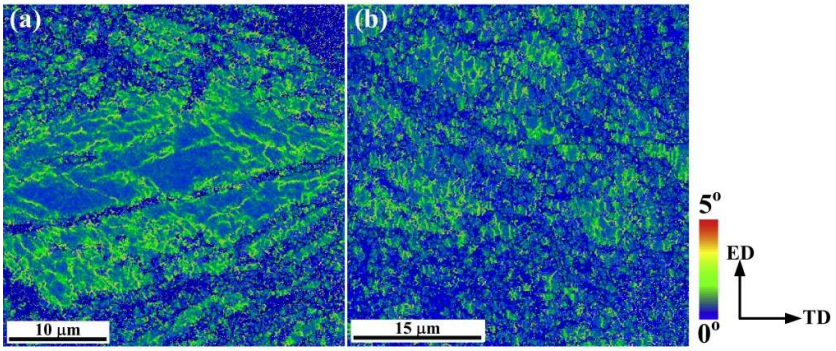

Fig. 13. Representative KAM maps of ECAPed Al–7Mg samples annealed at: (a) 200 °C for 30 min and (b) 275 °C for 8 h.

Furthermore, the layer Mg segregation and/or cluster along GBs can retard grain growth and hence enhance the thermal stability of nano/ultrafine grains via diminishing GB energy and dragging GBs. Similarly, the inhibited grain growth by Mg segregation via diminishing GB energy was evidenced in an as-sputtered Al–10Mg alloy [22], leading to nano-grains stabilized at 6.1 nm after annealing at 300 °C for 3 h. In addition, the present Al–7Mg alloy possesses a high solute Mg content, and the local concentrations of solute Mg atoms in some ultrafine grains even approach ~8.36 at.%, although the strong Mg segregation and/or clusters have been detected by APT analysis (Fig. 5). The high-content Mg atoms in solid solution can also contribute to the high thermal stability by retarding mobility of dislocations and GBs [37,46].

Moreover, Al_3Mg_2 precipitates at GBs are expected to impede GB migration during annealing. In general, the Al_3Mg_2 precipitation requires sufficient long time to overcome high nucleation barriers [1]. Meanwhile, Al_3Mg_2 precipitates are unstable during SPD, and it has been reported that Al_3Mg_2 precipitates produced by prior annealing were sheared by ECAP, leading to Mg being dissolved into an Al–3Mg alloy [38]. It may partially explain the results in present work that no Al_3Mg_2 phase has been revealed in the severely as-deformed sample (Figs. 3 and 4). Nevertheless, the low-temperature annealing for long time favours Al_3Mg_2 nucleation and growth by establishing a steady state [1]. Furthermore, solute segregation and/or clusters along GBs change the local thermodynamic state and enhance compositional

levels, which in principle accelerates the precipitation process along GBs, compared with grain interiors [36]. Accordingly, the Mg segregation and/or clusters along GBs allow Al_3Mg_2 to precipitate almost exclusively along GBs in the 200 ºC-annealed sample, which further contributes to stabilize the nano/ultrafine grains by pinning GBs.

5. Conclusions

We demonstrate that the multimodal-grained ECAPed high solid solution Al–7Mg alloy possesses enhanced thermal stability in comparison to dilute ultrafine-grained SPD-processed Al–Mg alloys in present work. When annealed at moderate to high temperatures, i.e. at 200 and 275 ºC, dislocation recovery and rearrangement occur preferentially; meanwhile, the nano/ultrafine grains grow sluggishly. The growth exponent of those ultrafine grains for 200 and 275 °C-annealed Al–7Mg samples reaches to ~3.9 and ~3.5, respectively, further demonstrating the high thermal stability, in comparison to the ultrafine grains in dilute Al–Mg alloys with a uniform microstructure. The enhanced thermal stability is mainly due to the multimodal grain structure, the strong solute Mg segregation and/or clusters and nanoscaled Al_3Mg_2 particles precipitating during the long-time annealing. First, when annealed at moderate to high temperatures, the extensive recovery over recrystallization consumes most of stored energy in both coarse grains and nano/ultrafine grains of the ECAPed Al–7Mg alloy, which retards or postpones recrystallization and growth behaviors of nano/ultrafine grains. Secondly, the Mg segregation and/or clusters can retard GB migration by decreasing GB energy and dragging GBs. Finally, Al_3Mg_2 precipitates forming during the long-time annealing could inhibit grain growth by pinning GBs, further improving the thermal stability. This study provides an alternative route, i.e. a multimodal grain structure combined with Mg solute segregation and/or clusters, to design SPD-processed high performance Al–Mg alloys with enhanced thermal stability.

Acknowledgements

Financial supports from The Natural Science Foundation of China (Nos. 51625402, 51922048, 51790483 and 51871108) are greatly acknowledged. Partial financial support comes from The Changjiang Scholars Program (T2017035).

References

[1] X. Sauvage, N. Enikeev, R. Valiev, Y. Nasedkina, M. Murashkin, Atomic-scale analysis of the segregation and precipitation mechanisms in a severely deformed Al-Mg alloy, Acta Mater. 72 (2014) 125–136.

[2] Y. Zhao, M.N. Polyakov, M. Mecklenburg, M.E. Kassner, A.M. Hodge, The role of grain boundary plane orientation in the β phase precipitation of an Al-Mg alloy, Scr. Mater. 89 (2014) 49–52.

[3] Y. Liu, M. Liu, X. Chen, Y. Cao, H.J. Roven, M. Murashkin, R.Z. Valiev, H. Zhou, Effect of Mg on microstructure and mechanical properties of Al-Mg alloys produced by high pressure torsion, Scr. Mater. 159 (2019) 137–141.

[4] M. Jobba, R.K. Mishra, M. Niewczas, Flow stress and work-hardening behaviour of Al-Mg binary alloys, Int. J. Plast. 65 (2015) 43–60.

[5] D. Zhao, O.M. Løvvik, K. Marthinsen, Y. Li, Impurity effect of Mg on the generalized planar fault energy of Al, J. Mater. Sci. 51 (2016) 6552–6568.

[6] J. Xue, S. Jin, X. An, X. Liao, J. Li, G. Sha, Understanding formation of Mg-depletion zones in Al-Mg alloys under high pressure torsion, J. Mater. Sci. Technol. 35 (2019) 858–864.

[7] Y. Tang, W. Goto, S. Hirosawa, Z. Horita, S. Lee, K. Matsuda, D. Terada, Concurrent strengthening of ultrafine-grained age-hardenable Al-Mg alloy by means of high-pressure torsion and spinodal decomposition, Acta Mater. 131 (2017) 57–64.

[8] H.R. Peng, M.M. Gong, Y.Z. Chen, F. Liu, Thermal stability of nanocrystalline materials: thermodynamics and kinetics, Int. Mater. Rev. 62 (2017) 303–333.

[9] M. Saber, C.C. Koch, R.O. Scattergood, Thermodynamic grain size stabilization models: An overview, Mater. Res. Lett. 3 (2015) 65–75.

[10] Q. Li, J. Cho, S. Xue, X. Sun, Y. Zhang, Z. Shang, H. Wang, X. Zhang, High temperature thermal and mechanical stability of high-strength nanotwinned Al alloys, Acta Mater. 165 (2019) 142–152.

[11] C. Meng, W. Hu, S. Sandlöbes, S. Korte-Kerzel, G. Gottstein, The effect of large plastic deformation on elevated temperature mechanical behavior of dynamic strain aging Al-Mg alloys, Acta Mater. 181 (2019) 67–77.

[12] H. Hasegawa, S. Komura, A. Utsunomiya, Z. Horita, M. Furukawa, M. Nemoto, T.G. Langdon, Thermal stability of ultrafine-grained aluminum in the presence of Mg and Zr additions, Mater. Sci. Eng. A. 265 (1999) 188–196.

[13] M.A. Atwater, D. Roy, K.A. Darling, B.G. Butler, R.O. Scattergood, C.C. Koch, The thermal stability of nanocrystalline copper cryogenically milled with tungsten, Mater. Sci. Eng. A. 558 (2012) 226–233.

[14] P. Choi, M. Da Silva, U. Klement, T. Al-Kassab, R. Kirchheim, Thermal stability of electrodeposited nanocrystalline Co-1.1at.%P, Acta Mater. 53 (2005) 4473–4481.

[15] B.K. VanLeeuwen, K.A. Darling, C.C. Koch, R.O. Scattergood, B.G. Butler, Thermal stability of nanocrystalline Pd81Zr19, Acta Mater. 58 (2010) 4292–4297.
[16] W. Xu, X.C. Liu, X.Y. Li, K. Lu, Deformation induced grain boundary segregation in nanolaminated Al–Cu alloy, Acta Mater. 182 (2020) 207–214.
[17] R.K. Koju, Y. Mishin, Atomistic study of grain-boundary segregation and grain-boundary diffusion in Al-Mg alloys, Acta Mater. 201 (2020) 596–603.
[18] D. Zhao, O.M. Løvvik, K. Marthinsen, Y. Li, Segregation of Mg, Cu and their effects on the strength of Al Σ5 (210)[001] symmetrical tilt grain boundary, Acta Mater. 145 (2018) 235–246.
[19] Y. Zhang, S. Jin, P.W. Trimby, X. Liao, M.Y. Murashkin, R.Z. Valiev, J. Liu, J.M. Cairney, S.P. Ringer, G. Sha, Dynamic precipitation, segregation and strengthening of an Al-Zn-Mg-Cu alloy (AA7075) processed by high-pressure torsion, Acta Mater. 162 (2019) 19–32.
[20] Y. Zhang, S. Jin, P. Trimby, X. Liao, M.Y. Murashkin, R.Z. Valiev, G. Sha, Strengthening mechanisms in an ultrafine-grained Al–Zn–Mg–Cu alloy processed by high pressure torsion at different temperatures, Mater. Sci. Eng. A. 752 (2019) 223–232.
[21] R.Z. Valiev, Superior Strength in Ultrafine-Grained Materials Produced by SPD Processing, Mater. Trans. 55 (2014) 13–18.
[22] A. Devaraj, W. Wang, R. Vemuri, L. Kovarik, X. Jiang, M. Bowden, J.R. Trelewicz, S. Mathaudhu, A. Rohatgi, Grain boundary segregation and intermetallic precipitation in coarsening resistant nanocrystalline aluminum alloys, Acta Mater. 165 (2019) 698–708.
[23] X. Sauvage, G. Wilde, S. V. Divinski, Z. Horita, R.Z. Valiev, Grain boundaries in ultrafine grained materials processed by severe plastic deformation and related phenomena, Mater. Sci. Eng. A. 540 (2012) 1–12.
[24] Y. Wang, M. Chen, F. Zhou, E. Ma, High tensile ductility in a nanostructured metal, Nature. 419 (2002) 912–915.
[25] M. Zha, Y. Li, R.H. Mathiesen, H.J. Roven, High ductility bulk nanostructured Al–Mg binary alloy processed by equal channel angular pressing and inter-pass annealing, Scr. Mater. 105 (2015) 22–25.
[26] M. Zha, Y. Li, R.H. Mathiesen, R. Bjørge, H.J. Roven, Achieve high ductility and strength in an Al–Mg alloy by severe plastic deformation combined with inter-pass annealing, Mater. Sci. Eng. A. 598 (2014) 141–146.
[27] M. Zha, Y. Li, R.H. Mathiesen, R. Bjørge, H.J. Roven, Microstructure evolution and mechanical behavior of a binary Al-7Mg alloy processed by equal-channel angular pressing, Acta Mater. 84 (2015) 42–54.
[28] Y.J. Chen, Y.C. Chai, H.J. Roven, S.S. Gireesh, Y.D. Yu, J. Hjelen, Microstructure and mechanical properties of Al-xMg alloys processed by room temperature ECAP, Mater. Sci. Eng. A. 545 (2012) 139–147.
[29] H. Pan, R. Kang, J. Li, H. Xie, Z. Zeng, Q. Huang, C. Yang, Y. Ren, G. Qin, Mechanistic investigation of a low-alloy Mg–Ca-based extrusion alloy with high strength–ductility synergy, Acta Mater. 186 (2020) 278–290.
[30] M. Liu, H.J. Roven, X. Liu, M. Murashkin, R.Z. Valiev, T. Ungár, L. Balogh, Grain refinement in nanostructured Al-Mg alloys subjected to high pressure torsion, J. Mater. Sci. 45 (2010) 4659–4664.
[31] J. Gubicza, N.Q. Chinh, J.L. Lábár, S. Dobatkin, Z. Hegedus, T.G. Langdon, Correlation between microstructure and mechanical properties of severely deformed metals, J. Alloys Compd. 483 (2009) 271–274.
[32] J. Gubicza, N.Q. Chinh, Z. Horita, T.G. Langdon, Effect of Mg addition on microstructure and mechanical properties of aluminum, Mater. Sci. Eng. A. 387-389 (2004) 55–59.

[33] M. Zha, X.-T. Meng, H.-M. Zhang, X.-H. Zhang, H.-L. Jia, Y.-J. Li, J.-Y. Zhang, H.-Y. Wang, Q.-C. Jiang, High strength and ductile high solid solution Al–Mg alloy processed by a novel hard-plate rolling route, J. Alloys Compd. 728 (2017) 872–877.
[34] R.Z. Valiev, N.A. Enikeev, M.Y. Murashkin, V.U. Kazykhanov, X. Sauvage, On the origin of the extremely high strength of ultrafine-grained Al alloys produced by severe plastic deformation, Scr. Mater. 63 (2010) 949–952.
[35] W.H. H.J. Axon, The lattice spacing of solid solutions of different elements in aluminium, Proc. R. Soc. A. 193 (1948) 1–24.
[36] H. Zhao, F. De Geuser, A. Kwiatkowski da Silva, A. Szczepaniak, B. Gault, D. Ponge, D. Raabe, Segregation assisted grain boundary precipitation in a model Al-Zn-Mg-Cu alloy, Acta Mater. 156 (2018) 318–329.
[37] M. Zha, Y. Li, R.H. Mathiesen, R. Bjørge, H.J. Roven, Annealing response of binary Al-7Mg alloy deformed by equal channel angular pressing, Mater. Sci. Eng. A. 586 (2013) 374–381.
[38] D.G. Morris, M.A. Muñoz-Morris, Microstructure of severely deformed Al-3Mg and its evolution during annealing, Acta Mater. 50 (2002) 4047–4060.
[39] M.A. Muñoz-Morris, C. Garcia Oca, G. Gonzalez-Doncel, D.G. Morris, Microstructural evolution of dilute Al-Mg alloys during processing by equal channel angular pressing and during subsequent annealing, Mater. Sci. Eng. A. 375-377 (2004) 853–856.
[40] Y.B. Lee, D.H. Shin, K.-T. Park, W.J. Nam, Effect of annealing temperature on microstructures and mechanical properties of a 5083 Al alloy deformed at cryogenic temperature, Scr. Mater. 51 (2004) 355–359.
[41] I. Roy, M. Chauhan, E.J. Lavernia, F.A. Mohamed, Thermal stability in bulk cryomilled ultrafine-grained 5083 Al alloy, Metall. Mater. Trans. A. 37 (2006) 721–730.
[42] B. Gwalani, R. Salloom, T. Alam, S.G. Valentin, X. Zhou, G. Thompson, S.G. Srinivasan, R. Banerjee, Composition-dependent apparent activation-energy and sluggish grain-growth in high entropy alloys, Mater. Res. Lett. 7 (2019) 267–274.
[43] F.J. Humphreys, M. Hatherly, Recrystallization and Related Annealing Phenomena (Second Edition), Elsevier, 2004.
[44] H.K. Zhang, H. Xiao, X.W. Fang, Q. Zhang, R.E. Logé, K. Huang, A critical assessment of experimental investigation of dynamic recrystallization of metallic materials, Mater. Des. 193 (2020) 108873.
[45] K. Huang, K. Marthinsen, The effect of heating rate on the softening behaviour of a deformed Al-Mn alloy with strong and weak concurrent precipitation, Mater. Charact. 110 (2015) 215–221.
[46] Y. Huang, F.J. Humphreys, The effect of solutes on grain boundary mobility during recrystallization and grain growth in some single-phase aluminium alloys, Mater. Chem. Phys. 132 (2012) 166–174.

Table captions:

Table 1. Lattice parameters estimated from XRD data by using a least squares refinement. Compared with the Mg content in as-homogenized condition, the loss of Mg (ΔMg) in as-ECAPed and annealed Al–7Mg samples is also included.

Samples	Lattice parameter (Å)	ΔMg (wt.%)
As-homogenized	4.0860±0.0002	-
As-ECAPed	4.0810±0.0001	0.96
200 °C-24 h	4.0735±0.0003	2.42
250 °C-30 min	4.0747±0.0001	2.19
275 °C-75 min	4.0778±0.0002	1.59
300 °C-30 s	4.0840±0.0001	0.38